HETEROCYCLES, Vol. 104, No. 2, 2022, pp. 288 - 309. © 2022 The Japan Institute of Heterocyclic Chemistry
Received, 18th October, 2021, Accepted, 10th November, 2021, Published online, 19th November, 2021
DOI: 10.3987/COM-21-14573

DESIGN AND SYNTHESIS OF NEW QUINOLINE LINKED TO PYRANOTRIAZOLOPYRIMIDINES CONJUGATES AS NOVEL TARGETS TO DISCOVER PROMISING ANTI-SARS-COV-2

Faisal K. Algethami,[1]* Salma Jlizi,[2] Mansour Znati,[2] Naoufel Ben Hamadi,[1,2] Anis Romdhane,[2] Mohamed R. Elamin,[1] Lotfi Khezami,[1] and Hichem Ben Jannet[2]*

[1]Department of Chemistry, College of Science, Imam Mohammad Ibn Saud Islamic University (IMSIU), Riyadh 11432, Saudi Arabia; E-mail: falgethami@imamu.edu.sa

[2]Laboratory of Heterocyclic Chemistry, Natural Products and Reactivity (LR11ES39), Team: Medicinal Chemistry and Natural Products, Faculty of Science of Monastir, University of Monastir, Avenue of Environment, 5019 Monastir, Tunisia; E-mail: hichem.bjannet@gmail.com

Abstract – Simple one-pot synthesis of 2-aminopyranoquinoline-3-carbonitriles **2a-d** at room temperature from available 8-hydroxyquinaldine, malononitrile, and substituted aromatic aldehydes was realized. Compounds **2a-d** were converted into imino ethers **3a-d**, condensed with a series of hydrazide under microwave irradiation to yield novel pyranotriazolopyrimidines fused to quinoline **4a-f**. Compound **4c**, with a cyanomethyl group, was treated with some salicylic arylaldehydes to give the corresponding new pyranotriazolopyrimidine-chromen hybrids **5a-c** in good yields. Finally a new series of arylidenes linked to triazolopyrimidopyrano[3,2-*h*]quinoline **6a-h** were designed and synthesized by the reaction of **4a,c**, both bearing a cyanomethyl group, with a series of arylaldehydes. The structures of all the compounds were evidenced by $^{1}H/^{13}C$ NMR, IR, and ESI-HRMS. The present study focuses also to predict the theoretical assembly of the COVID-19 protease (SARS-CoV-2 M^{pro}) and to find in advance whether this protein can be targeted by the compounds **4c**, **4f**, **5a-c** and **6a-h** thus synthesized. The docking scores of these compounds were compared to that of the co-crystallized native ligand inhibitor (N3) used as a reference standard.

The results showed that all the synthesized compounds (**4c**, **4f**, **5a-c** and **6a-h**) gave interesting binding scores compared to the N3 inhibitor. It has been found that compounds **4c**, **4f**, **5a** and **5b** achieved considerably similar binding scores and modes of interaction than the co-crystallized inhibitor N3 indicating good affinity towards SARS-CoV-2 M^{pro}. Conversely, the derivatives **6h** and **5c** showed binding energy scores (-8.9 and -8.8 kcal/mol, respectively) higher than the M^{pro} N3 inhibitor (-7.0 kcal/mol), revealing, in their turn, strong interaction with the target protease. However, their interactions were not entirely comparable to those of reference N3.

INTRODUCTION

Coronaviruses constitue a group of multiple viruses that infect several animals, and sometimes cause certain respiratory infections in humans. In 2019, a new coronavirus called SARS-CoV-2 appeared in Wuhan (China), and caused an epidemic of viral pneumonia that humanity has never experienced before. This highly transmissible disease (COVID-19) has affected the whole world.[1,2]

Moreover, the source of this virus, its behavior and its mode of pathogenesis, poorly understood until now, gave the kick-off to several research teams around the world in chemistry, biology, pharmacology and medicine to discover vaccines and anti-SARS-CoV-2 drugs, and consequently save the humanity from this dramatic infectious disease. In this context, the researchers aimed to discover new anti-covid-19 by exploiting the existing antiviral compounds that could fight the infection based on *silico* predictions.

On the other hand, as defined in previous works, advantageous molecules are chemical entities characterized by polyvalent binding properties, which allow it possible to make these molecules vigorous and specific ligands for a broad spectrum of biological targets *via* appropriate chemical modifications.[3,4] Among these privileged entities, quinoline derivatives are very well cited in the literature for their various biological potentials such as antialzheimer,[5] anticancer,[6-8] anti-HIV,[9,10] anti-schistosomal[11] and antiviral (Figure 1-A,[12] Figure 1-B[13]).

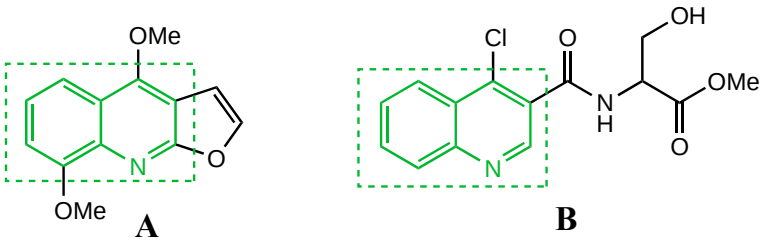

Figure 1

Furthermore, many clinically accepted drugs such as mefloquine,[14] gatifloxacin,[15] sitafloxacin,[16] and garfenoxacin[17] contain quinoline as their core pharmacophore.

On the other hand, heterocyclic systems with pyran and benzopyran moieties constitute an excellent category of compounds endowed with a broad spectrum of therapeutic effects. They have been reported to exhibit several potentials such as antimicrobial,[18] anticoagulant, antit-tyrosinase,[19] α-amylase,[20] anti-soybean lipoxygenase, anti-xanthine oxidase, cytotoxic,[21] and antiviral activities (Figure 2-A,[22] Figure 2-B,[23] Figure 2-C[24]).

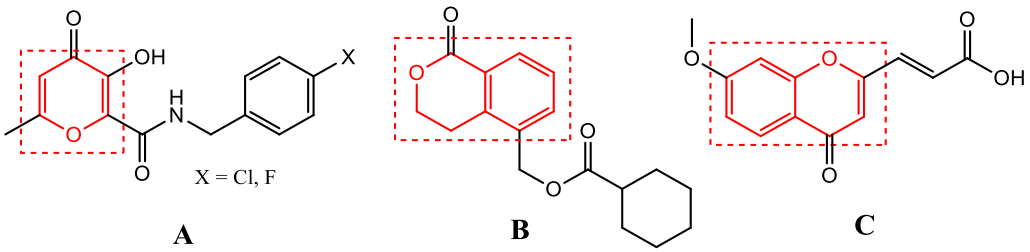

Figure 2

Moreover, it has been reported that the incorporation of the triazolopyrimidine moiety into organic molecules has been developed in recent years due to its varied effects in various biological domains. In addition, the junction of the triazolopyrimidine ring with other heterocyclic systems leads to a new class of polyheterocyclic compounds with more interesting biological activities including anti-acetylcholinesterase,[25] anti-xanthine oxidase,[21] anticancer,[26] antiproliferative,[27] and antiviral (Figure 3-A,[28] Figure 3-B,[29] Figure 3-C[30]).

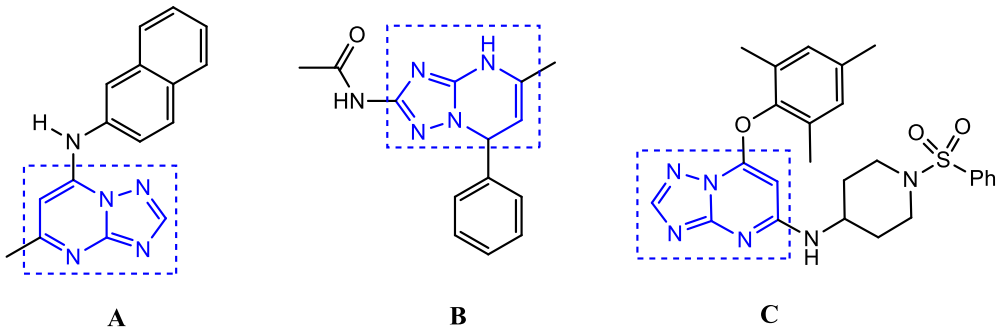

Figure 3

In addition, the literature review showed that numerous target-based screenings were performed to discover promising protease inhibitors against SARS-CoV-2. Among them, some derivatives incorporating in their structures are respectively cited: quinoline (Figure 4-A),[31] pyran (Figure 4-B)[32] and triazolopyrimidine moities (Figure 4-C).[33]

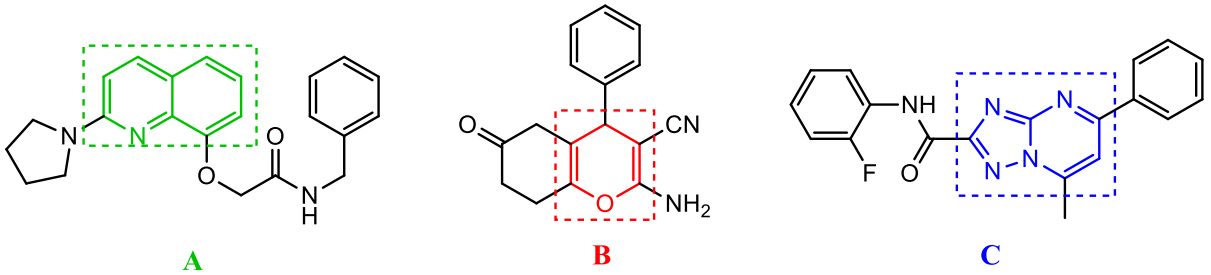

Figure 4

The structural linkage of several pharmacophores has been extensively studied by several research teams around the world including our team, with the aim of designing and synthesizing new and better active principles. This idea of linkage of different fragments reputed to be responsible for the biological effect of the molecule that they constitute has led in several cases to interesting results showing the effect of synergy between the different scaffolds introduced into the same molecule to built a new pharmacophore with more powerful activity.[20,34-37]

To our knowledge, no work has been described in the literature concerning the connection between the quinoline and pyranotriazolopyrimidine fragments. The different scaffolds introduced above (quinoline, pyran and triazolopyrimidine) as anti-SARS-CoV-2 pharmacophores encouraged us to introduce them into the same molecule to react if possible in synergy against the SARS-CoV-2 virus.

In this context, and in the continuity of looking for new bioactive compounds,[19-21,25,38,39] where in the preparation of a new series of fused compounds **4**, consisting of fragments assigned as antiviral and anti-SARS-CoV-2 agents as indicated above, such as quinoline, pyran and triazolopyrimidine systems *via* cyclocondensation reaction are reported. This approach can perform their virtual screening, using molecular docking studies, hoping to find promising protease inhibitors against COVID-19.

RESULTS AND DISCUSSION

According to literature procedure,[40] the starting materials 2-aminopyranoquinoline-3-carbonitriles **2a-d** were easily obtained *via* one-pot multicomponent reactions of arylaldehyde, malononitrile and 8-hydroxyquinaldine in the presence of K_2CO_3. *α*-Functionalized imino ethers **3a-d** were prepared by treating **2a-d** with triethyl orthoformate in acetic anhydride at refluxing temperature (Scheme 1).

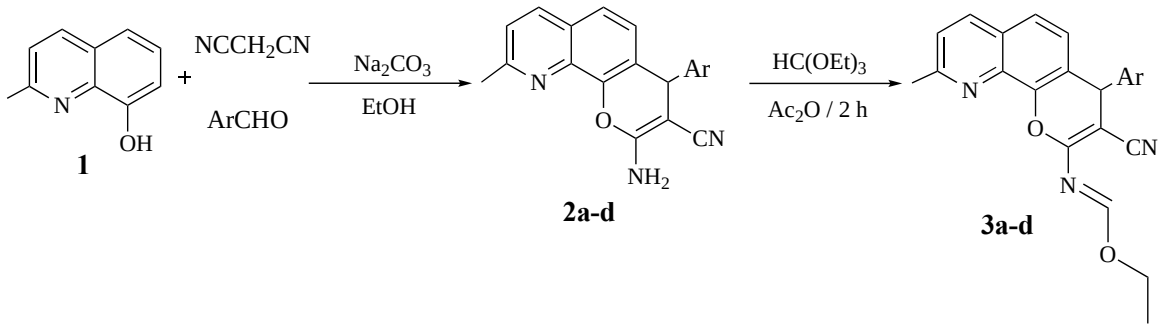

Comp.	Ar	Yiled (%)
2a	Ph	81
2b	*p*-Cl-Ph	75
2c	*p*-Me-Ph	85
2d	*p*-MeO-Ph	70

Scheme 1. Synthetic route of compounds **3a-d**

Although the yields for obtaining compounds **2a-d** are calculated after washing with hot water and ethanol, we have found that the donor groups by +M effects (Cl and OMe) carried by the arlyaldehydes **2b** and **2d**, respectively slightly disadvantaged the nucleophilic addition of the formed malononitrile carbanion to the carbonyl, thus leading to relatively low yields compared to those of **2a** and **2c**. The slightly high yield of obtaining the chlorinated derivative **2b** compared to that of **2d** (OMe) is explained by the -I effect of the chlorine atom which opposes its +M effect, and consequently increases the electrophilic ability of carbonyl.

Prompted by the varied biological activities of triazolopyrimidines derivatives,[25-30,38,39] the synthesis of new pyranotriazolopyrimidines fused to quinoline using microwave irradiation assistance was also described. Indeed, the imidates **3a**,**b**, the most stable from the series **3a-d**, were selected to be treated, without any previous purification, with some hydrazides in anhydrous DMF for 5 to 9 minutes under microwave irradiation at 350 W to furnish the new 1,2,4]triazolo[1'',5'':1',6']pyrimido[5',4':5,6]pyrano[3,2-*h*]quinolines **4a-f** (Scheme 2). Mechanistically, the reaction begins with a first nucleophilic attack of the primary amine group of hydrazide on the sp2 carbon of the iminoether moiety. The non-isolable intermediate formed undergoes cyclization by nucleophilic addition to the cyano function, thus generating the intermediates **3'a-f**. Finally, the intermediates **3'a-f** undergo an intracyclisation *via* eliminating a molecule of water to give triazolopyrimidopyrano-[3,2-*h*]quinoline **4a-f** in good to excellent yields (75-82%) (Scheme 2). The latter were calculated after recrystallization from ethanol of each product. The slight difference between these values is certainly due to the nature of the R group, the electronic effect of which influences the attack of the imine nitrogen

doublet on the carbonyl, let us cite the example of compound **4c** carrying a -CH_2CN exerting an attractor effect (-I) which promotes nucleophilic attack on the carbonyl in the intermediate 3'.

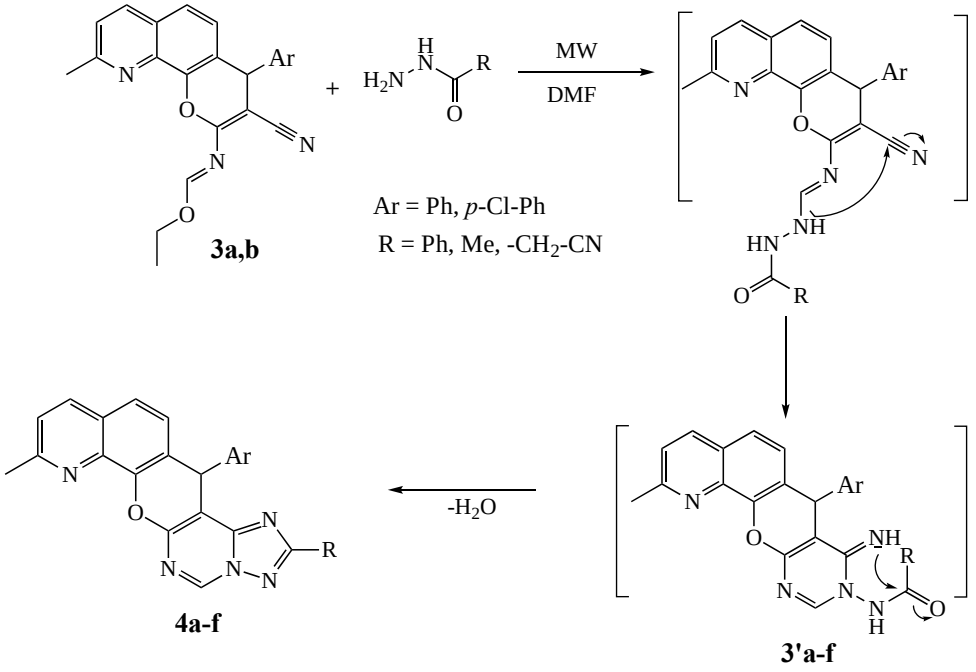

Comp.	R	Ar	Yiled (%)
4a	Me	Ph	75
4b	Ph	Ph	75
4c	-CH_2CN	Ph	78
4d	Me	*p*-Cl-Ph	82
4e	Ph	*p*-Cl-Ph	75
4f	-CH_2CN	*p*-Cl-Ph	75

Scheme 2. Plausible mechanistic pathway for the access to derivatives **4a-f**

The structures of derivatives **4a-f** were determined with the help of their spectra (IR, ^{1}H NMR, ^{13}C NMR, and ESI-HRMS). Their IR spectra displayed the non-existence of the characteristic absorption bands corresponding to cyano, amino and carbonyl functions. In addition, ^{1}H NMR spectra of **4a-f** did not show the signals of the ethoxy group in **3a,b**, the appearance of signals at δ_H 7.13-8.27 relating to the protons of quinoline and aryl moieties, a singlet at δ_H 5.81-5.94 attributable to the proton of the pyran ring, as well as a singlet at 9.04-9.14 corresponding to the unique proton of the pyrimidine fragment. The ^{13}C NMR spectra of these compounds revealed all the expected carbon signals such as those introduced by the hydrazides used. ESI-HRMS spectra of the prepared compounds were also found to be consistent with their structures.

In the compounds **4c** and **4f**, mentioned above, the cyanomethyl moiety made them valuable key precursors for the formation of several heterocyclic compounds[38,41-43] and aroused our interest to explore them in order to obtain the desired hybrid compounds **5** and **6**. In this context, and according of some previous work,[25,44-46] we reacted compound **4c** (Ar=Ph) with three salicylic arylaldehydes under reflux of ethanol in the presence of piperidine for 12 h leading to the new pyranotriazolopyrimidine-chromen conjugates **5a-c** (Scheme 3) in yields ranging from 72 to 79%. The relatively high yield of derivative **5c** (79%) is easily explained by the attractor effects -I and -M exerted by the NO_2 group which favors the attack on the carbonyl function of the aryldehyde. The IR spectra of these derivatives showed the absence of CN absorption bands of the precursor **4c** and the presence of chromen -C=NH absorption bands at 1679-1690 cm^{-1}. In addition to signals of aromatic protons, their ^1H NMR spectra displayed a supplementary signal with those of the protons of aromatic moieties at δ_H 7.10-8.25 attributable to the iminic NH proton and the disappearance of signals assignable to the methylene group. Compounds **5a-c** structures were also evidenced by their ^{13}C NMR spectra showing new signals relating to carbons of the salicylic aldehydes used. HR-MS data of the prepared compounds were found to be in accordance with the given structures.

In the last few years, the condensation reactions of Knoevenagel have been considered a chosen path for the preparation of highly diverse molecules.[47,48] In this regard, condensation of **4c** and **4f** with some aromatic aldehydes in the presence of piperidine in ethanol afforded the targeted arylidenes derivatives **6a-h** in yields ranging from 68 to 80% (Scheme 3). The fluctuation of these values, calculated after washing the precipitate formed with ethanol, is due to the inductive and mesomeric effects of the different groups carried by the aromatic ring Ar^1. Their structures were confirmed by their IR, ^1H NMR, ^{13}C and ES-HRMS spectral data. The IR spectra of **6a-h** were characterized by the presence of absorption bands within the 2220-2235 cm^{-1} region attributable to the CN group stretching vibrations. In addition, the ^1H NMR spectra did not show the singlet relative to the methylene protons but revealed a new singlet at δ_H 9.15-9.25 characteristic of the ethylenic proton $H_{3'}$. The ^{13}C NMR spectra showed the non-existence of the signal attributable to the methylene carbon, and the appearance of two new signals at δ_C 107.0-107.7 and 153.2-153.7 corresponding to the two carbons $C_{2'}$ and $C_{3'}$, respectively. The HR-MS data of all new arylidenes also confirmed the given structures.

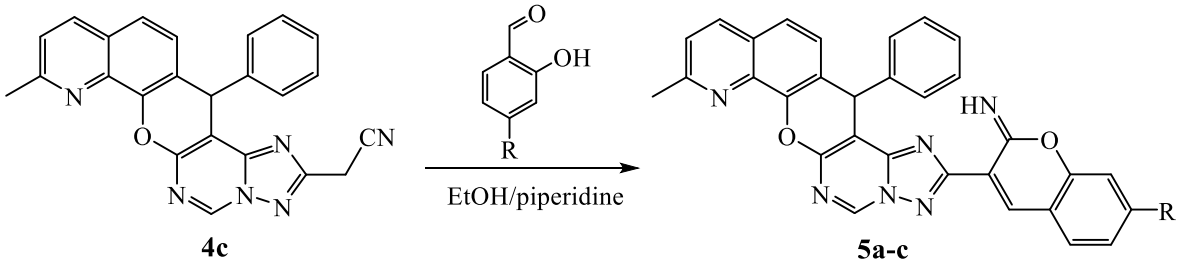

Comp.	R	Yiled (%)
5a	H	81
5b	Br	75
5c	NO_2	85

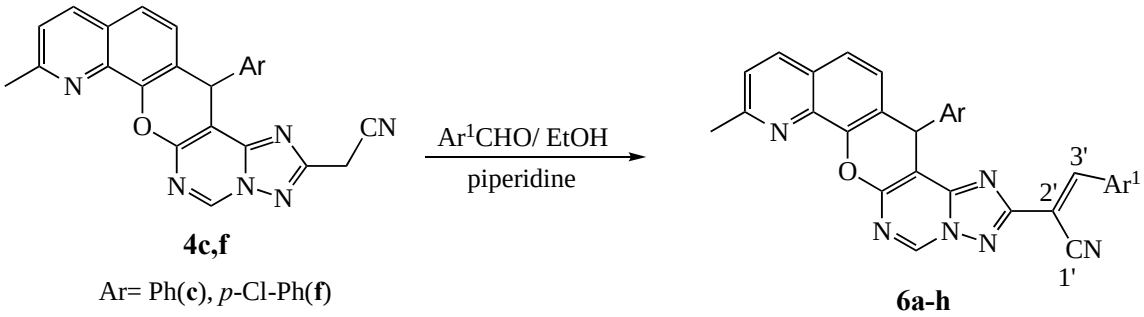

4c,f

Ar= Ph(**c**), *p*-Cl-Ph(**f**)

6a-h

Comp.	Ar	Ar^1	Yiled (%)
6a	Ph	Ph	70
6b	Ph	*p*-Me-Ph	73
6c	Ph	*p*-MeO-Ph	78
6d	Ph	*p*-$(Me)_2$N-Ph	80
6e	*p*-Cl-Ph	Ph	68
6f	*p*-Cl-Ph	*p*-Me-Ph	70
6g	*p*-Cl-Ph	*p*-MeO-Ph	75
6h	*p*-Cl-Ph	*p*-$(Me)_2$N-Ph	78

Scheme 3. Synthetic pathway for the compounds **5a-c** and **6a-h**

Docking study

The study of the binding pocket of the SARS-CoV-2 M^{pro}, pointed that the co-crystallized native inhibitor (N3) is located inside the pocket of the main protease receptor with an asymmetric view.[49] The N3 ligand is a designed inhibitor for SARS-CoV-2 M^{pro} erect from amino acids based on the M^{pro} pocket amino acids and cannot be used medicinally. The main residues in this pocket were MET-49, PHE-140, HIS-41, LEU-167, GLY-143, HIS-164, THR-190, MET-165, GLU-166, PRO-168, HIS-172, ALA-191 and GLN-189.

Molecular docking of the synthesized molecules (**4c**, **4f**, **5a-c**, and **6a-h**) and re-docked N3 inhibitor into the main protease binding site was performed. The binding energies and the interactions between the ligands and the target enzyme are displayed in Table 1.

All compounds were perfectly placed in the active site with variable scores and *via* binding interactions with the receptor pocket amino acids. From the docking results (Table 1), all the tested compounds (**4c**, **4f**,

5a-c and **6a-h**) achieved good binding scores ranging from -7.3 to -8.9 kcal/mol, compared to the docked co-crystallized N3 inhibitor with a binding score of -7.0 kcal/mol. The synthesized compounds (**4c**, **4f**, **5a-c** and **6a-h**) showed a much higher binding affinity towards the M^{pro} enzyme (PDB: 6LU7) than N3.

The main residues in the pocket were reported to be responsible for the significant energy.[50] From the docking results (Table 1), the amino acids MET-49, HIS-41, LEU-167, GLY-143, THR-190, MET-165, GLU-166, PRO-168, HIS-172, ALA-191 and GLN-189, interacted with most of the synthesized molecules (**4c**, **4f**, **5a-c**, and **6a-h**). This finding demonstrates that the synthesized molecules make multiple contacts with the residues in M^{pro} active pocket. Moreover, in addition to the different amino acids (MET-49, HIS-41, GLY-143, MET-165 and GLN-189) which interact with N3 in M^{pro} active pocket, the synthesized compounds exert further interactions with another series of amino acids (LEU-167, THR-190, GLU-166, PRO-168, HIS-172 and ALA-191) also present in the same active pocket. Most of the residues in the active site contribute significantly to the favorable interaction with the tested compounds and therefore the decrease in binding energy compared to docked N3.

It is worth mentioning that, especially for compounds **4f**, **5a**, **5b** and **4c**, the obtained binding modes were quite similar to that of the docked N3 inhibitor, but remain less than those shown by the crystallographic N3 as depicted in Table 2. Moreover, these four selected compounds exhibited binding scores of -8.9, -8.8, -8.8 and -8.1 kcal/mol, respectively, higher than of the docked co-crystallized N3 inhibitor (-7.0 kcal/mol) (Table 1).

The docked N3 inhibitor was stabilized inside the SARS-CoV-2 M^{pro} pocket through three hydrogen bonds formation with GLY-143, HIS-164 and GLN-198 amino acids with the bond lengths of 2.96, 2.67 and 3.25 Å, respectively. Also, it formed a pi-alkyl bond with MET-165 (bond length: 5.05 Å) and two alkyl interactions with HIS-41 (bond length: 4.28 Å) and MET-49 (bond length: 4.45 Å) residues. On another side, the compound **4f** fitted inside the binding site of the SARS-CoV-2 M^{pro} by a hydrogen bond formation, with GLN-192 at 3.15 Å, with an additional pi-sigma and carbon-hydrogen bonds with GLN-189 residue at 3.64 and 3.44 Å, respectively, two alkyl interactions with LEU-27 and HIS-41 at 4.34, 4.44 Å, respectively, and four pi-alkyl bonds with CYS-145 at 4.80 and 5.40 Å and MET-165 at 4.24 and 4.58 Å. Moreover, compound **5a** showed a hydrogen bond with the GLU-166 amino acid at 2.20 Å. Also, it showed two carbon-hydrogen bonds with GLN-189 (bond length: 3.40 Å) and THR-190 (bond length: 3.71 Å), a pi-sigma interaction with PRO-168 (bond length: 5.53 Å), a pi-pi T-shaped bond with HIS-41 (bond length: 4.49 Å), two alkyl interactions with HIS-41 (bond length: 5.45 Å) and MET-49 (bond length: 4.56 Å) and two pi-alkyl bonds with MET-49 (bond length: 4.57 Å) and PRO-168 (bond length: 4.75 Å) residues. In addition, the compound **5b** formed a hydrogen bond, two carbon hydrogen bonds, a pi-sigma interaction, a pi-pi T-shaped bond, two alkyl interactions and a pi-alkyl bond with the previously mentioned six amino acids as well. It formed a hydrogen bond with GLU-166 at 2.25 Å, two

carbon-hydrogen bonds with GLN-189 and THR-190 at 3.34 and 3.63 Å, respectively, a pi-sigma interaction with PRO-168 at 3.49 Å, a pi-pi T-shaped bond with HIS-41 at 4.47 Å, two alkyl interactions with HIS-41 and MET-49 at 4.56 and 4.54 Å, respectively, and two pi-alkyl bonds with MET-49 and PRO-168 at 4.54 and 4.77 Å, respectively. The compound **4c** was engaged in a hydrogen bond with GLN-192 (bond length: 3.22 Å), a carbon-hydrogen bond with GLN-189 (bond length: 3.51 Å), two alkyl interactions with LEU-27 (bond length: 5.43 Å) and HIS-41 (bond length: 4.68 Å) and two pi-alkyl bonds with MET-165 (bonds length: 4.29 and 4.51Å).

Although compounds **6h** and **5c** did not exhibit very comparable interactions to those of N3 towards SARS-CoV-2 M^{pro}, they, on the other hand, showed lower binding energy (-8.5 and -8.4 kcal/mol, respectively) (Table 1). This result can be interpreted, in part, by the nature of interactions between these compounds and the amino acids that constitute SARS-CoV-2 M^{pro} (Table 3). Indeed, the compound **6h** formed hydrogen bond with CYS-145 at 3.70 Å, a pi-pi T-shaped bond with HIS-41 (bond length: 5.29 Å), two alkyl interactions with LEU-27 (bond length: 3.55 Å) and HIS-41 (bond length: 4.39 Å) and five pi-alkyl bonds with CYS-145 (bonds length: 4.59 and 5.02 Å), MET-165 (bonds length: 4.64 and 5.14Å) and PRO-168 (bond length: 4.62 Å). The compound **5c** is interred in several interactions including two hydrogen bond, pi-anion bond, pi-pi T-shaped bond, amide-pi Stacked bond and three pi-alkyl bonds with the side chain residues HIS-41 (bond length: 2.80 Å), TYR-54 (bond length: 3.11 Å), GLU-166 (bond length: 3.53 Å), LEU-167 (bond length: 5.16 Å), HIS-41 (bond length: 5.52 Å), MET-165 (bond length: 4.67 Å), PRO-168 (bonds length: 4.97 and 5.20 Å), respectively.

According to these findings, the tested compounds, particularly **4c**, **4f**, **5a**, **5b**, **5c** and **6h**, could effectively act as novel antiviral agents against SARS-CoV-2.

Table 1. Binding energy (kcal/mol) and interactions of compounds **4c**, **4f**, **5a-c** and **6a-h** docked in the active site of M^{pro} enzyme (PDB: 6LU7).

Compound	Binding energy (kcal/mol)	Interaction: NI/NIAA: IAA
4c	-8.1	6/5: LEU-27, HIS-41, MET-165, GLN-189, GLN-192*
4f	-8.9	9/6: LEU-27, HIS-41, CYS-145, MET-165, GLN-189, GLN-192*
5a	-8.8	9/6: HIS-41, MET-49, GLU-166*, PRO-168, GLN-189, THR-190
5b	-8.8	9/6: HIS-41, MET-49, GLU-166*, PRO-168, GLN-189, THR-190
5c	-8.4	8/6: GLU-166, PRO-168, LEU-167, MET-165, TYR-54*, HIS-41*

6a	-7.9	6/4: THR-26*, HIS-41, ASN-142, CYS-145
6b	-8.2	5/3: THR-26*, ASN-142, CYS-145
6c	-8.2	8/6: GLY-143*, ALA-191, MET-165, PRO-168, CYS-145, ARG-188
6d	-7.9	5/3: THR-26*, ASN-142, CYS-145
6e	-7.3	9/6: THR-24*, THR-25*, THR-45*, MET-49, CYS-145, HIS-163
6f	-7.9	8/5: LEU-27, CYS-145, MET-165, PRO-168, ALA-191
6g	-8.2	8/6: GLY-143*, CYS-145, MET-165, PRO-168, ARG-188, ALA-191
6h	-8.5	9/5: LEU-27, HIS-41, CYS-145*, MET-165, PRO-168
N3	-7.0	6/6: HIS-41, MET-165, GLY-143*, HIS-164*, MET-49, GLN-189*

NI: Number of interactions, NIAA: Number of interacting amino acids, IAA: Interacting amino acids, *One hydrogen bond.

Table 2. 3D representations describe the binding interactions and positioning between the four selected compounds (**4f**, **5a**, **5b**, and **4c**) and the N3-binding pocket compared to the docked N3 inhibitor.

Code	3D Binding Interactions	3D Pocket Positioning
4f	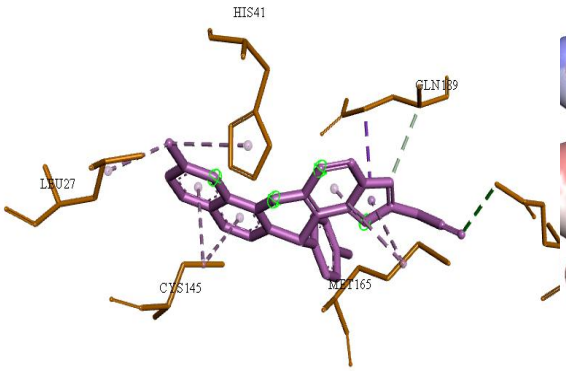	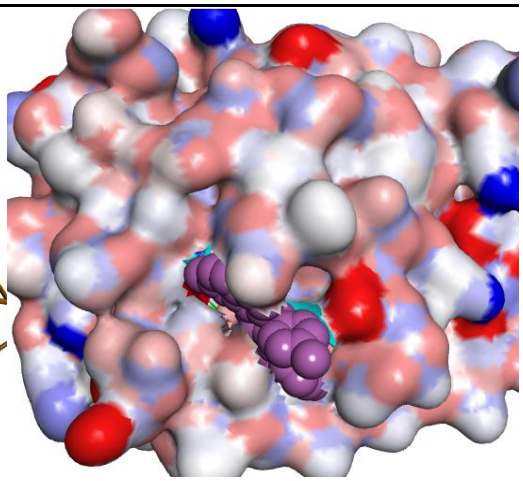

5a

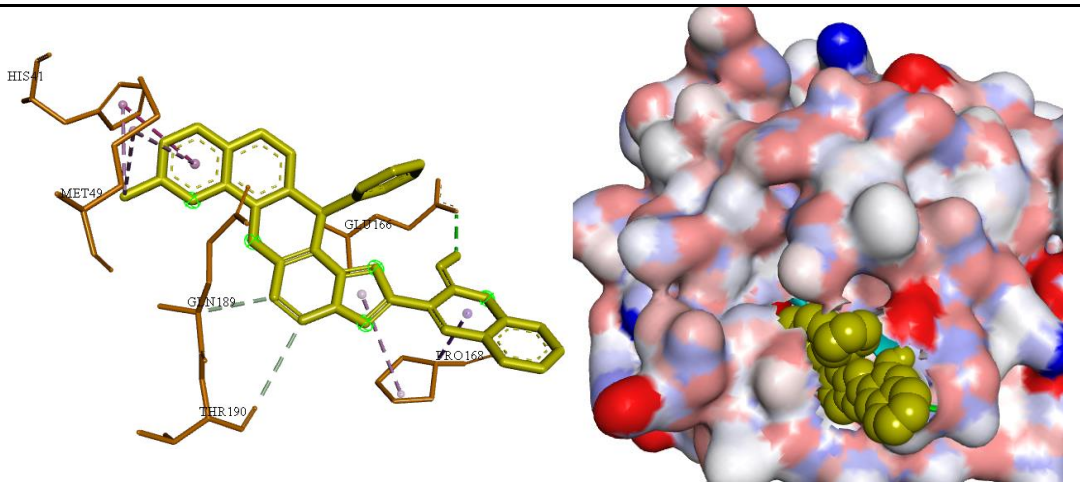
HIS41
MET49
GLU166
GLN189
PRO168
THR190

5b

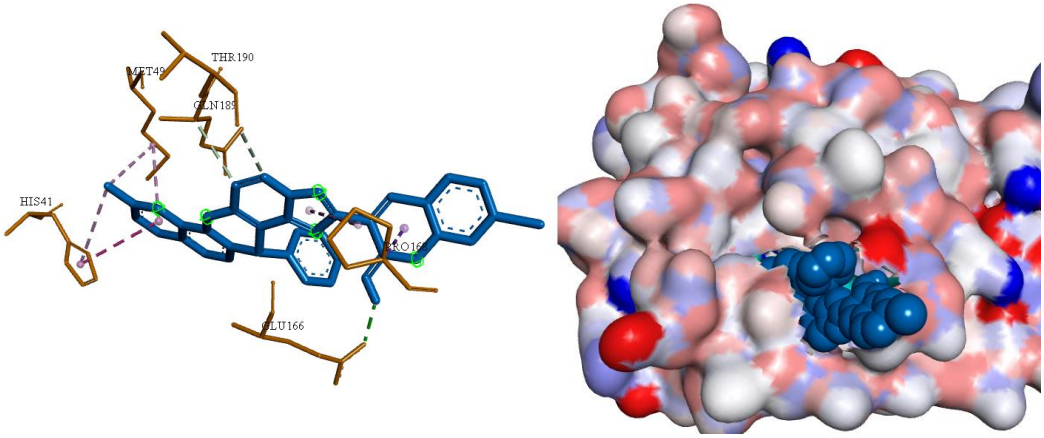
THR190
MET49
GLN189
HIS41
PRO168
GLU166

4c

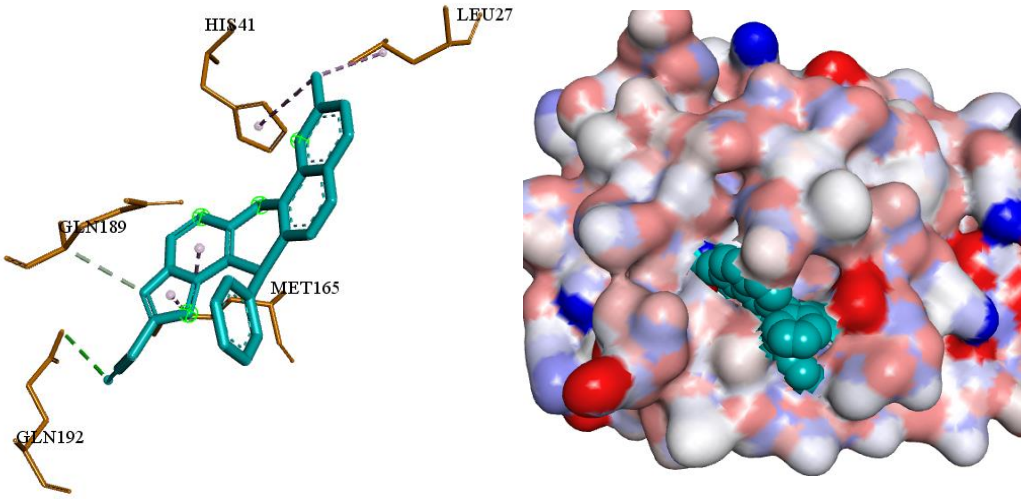
HIS41
LEU27
GLN189
MET165
GLN192

N3 (docked)	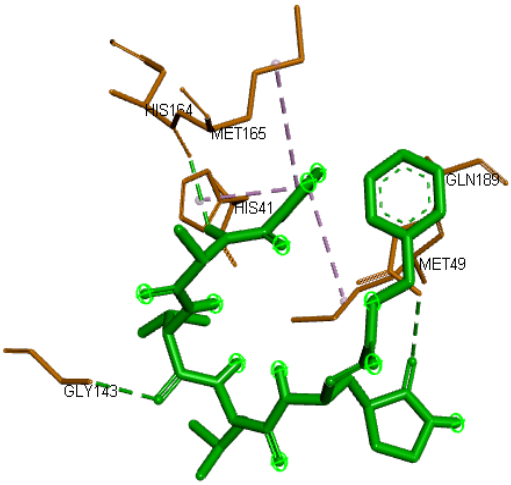	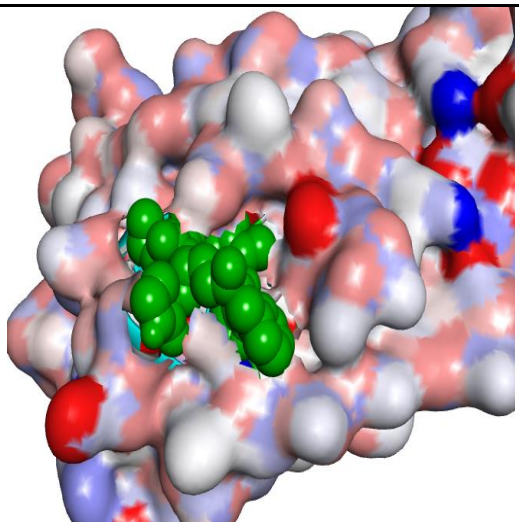
N3 (crystallographic form)	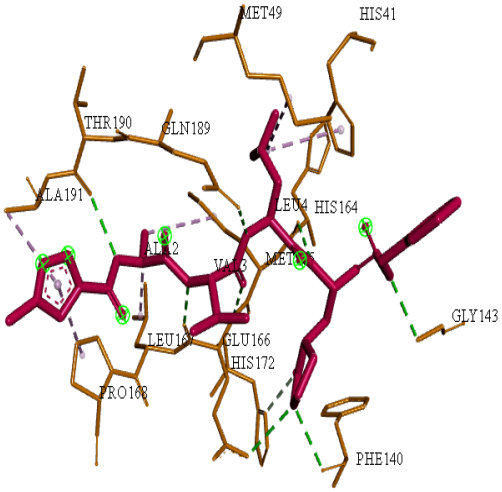	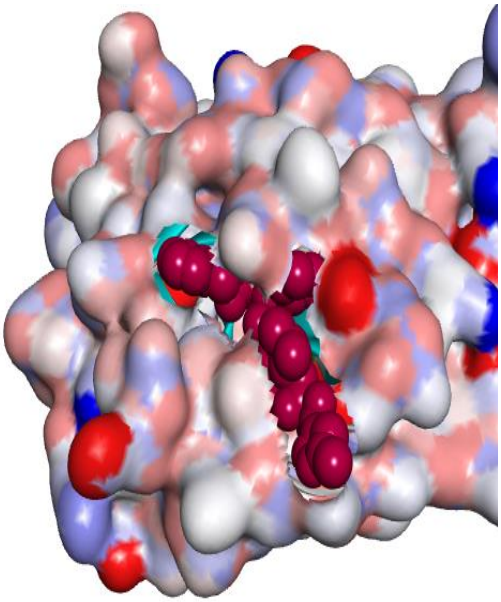

Table 3. 3D representations of the binding interactions and the location of the three compounds **6h** and **5c** in the N3 binding pocket.

Code	3D Binding Interactions	3D Pocket Positioning
6h	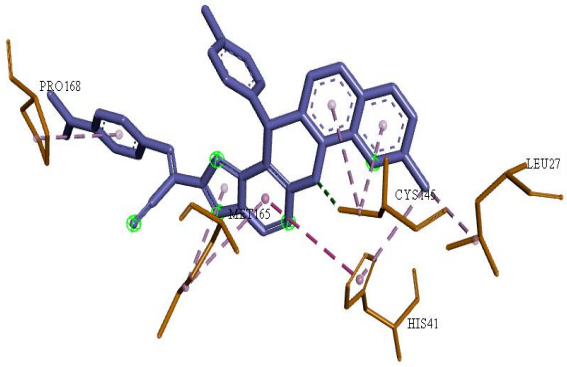	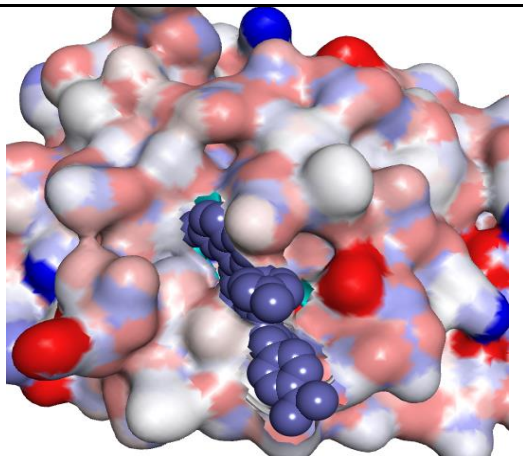
5c	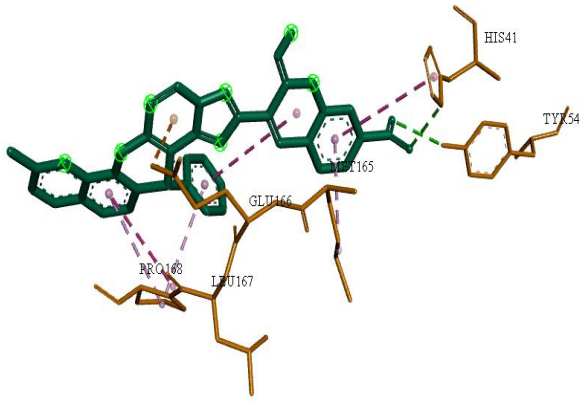	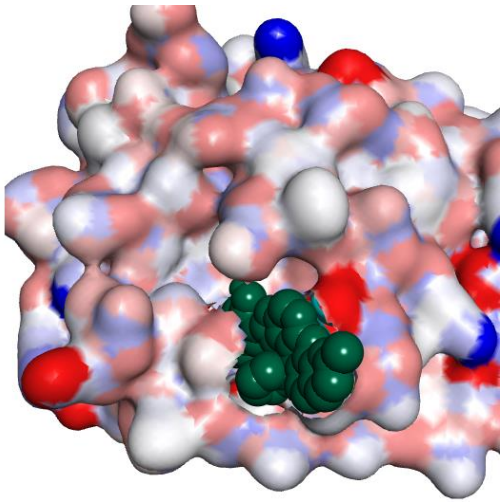

CONCLUSIONS

We have designed and successfully synthesized a series of new pyranotriazolopyrimidines fused to quinoline **4a-f** *via* condensation of imidates **3a**,**b** with some hydrazides. Then, new pyranotriazolopyrimidine-chromen hybrids **5a-f** were prepared from the reaction of compound **4b** containing cyanomethyl with salicylic aldehydes. Finally, we have described the access to new bioactive hybrid molecules **6a-h** has been described. Furthermore, the *in silico* docking studies showed that compounds **4c**, **4f**, **5a**, **5b**, **5c** and **6h** displayed a higher affinity for binding to the active site of M^{pro} than the native ligand (N3), and they could be considered as potential M^{pro} inhibitor candidates.

EXPERIMENTAL

Chemistry. All the reactions envisaged were verified by TLC on silica gel 60 F_{254} aluminum sheets, 0.2 mm (Merck). A StartSynth multimode microwave instrument ensuring a continuous microwave output power ranging from 0 to 1400 W was used (Milestone S.r.l., Sorisole, Italy). The melting temperatures were measured on an electrothermal device 9002 and were given without correction. NMR ^{1}H (300 MHz) and ^{13}C (75 MHz) spectra were run using a Bruker AC-300 spectrometer. The chemical shifts of protons and 13-carbons were given as δ values (ppm) relative to the residual solvent (non-deuterated). The ESI-HRMS were recorded on an LCT Premier XE mass spectrometer (Waters, ESI technique, positive mode). Compounds **3a,b** were used without prior purification for the synthesis of compounds **4a-f**. Attempts to have single crystals for performing X-ray diffraction analyzes failed for all compounds synthesized.

General experimental way for the preparation of derivatives 2a-d. A solution of arylaldehydes (10 mmol), malononitrile (10 mmol) and 8-hydroxyquinaldine (10 mmol) in the presence of sodium carbonate in EtOH was subjected to agitation at room temperature for 1 h. Once the reaction was over, compounds **2a-d** were obtained in solid form after filtration and washing with hot water and EtOH.

Compound (2a): White solid, yield: 81%, mp: 230-232 °C (EtOH); IR (KBr, cm^{-1}) υ: 3325-3450 (NH_2), 2217 (CN). ^{1}H NMR (300 MHz, $CDCl_3$) δ_H: 2.68 (s, 3H, CH_3), 4.91 (s, 1H, H-pyran), 5.01 (s, 2H, -NH_2), 7.07-8.18 (m, 9H, H_{arom}). ^{13}C NMR (75 MHz, $CDCl_3$) δ_C: 24.9, 41.3, 56.7, 118.3, 120.1, 121.2, 122.3, 124.3, 126.8, 127.5, 128.6, 130.0, 135.9, 137.1, 142.7, 151.0, 155.9, 166.4. ESI-HRMS $[M+H]^+$ calcd for $(C_{20}H_{16}N_3O)^+$ 314.1290, found 314.1293.

Compound (2b): White solid, yield: 75%, mp: 228-230 °C (EtOH); IR (KBr, cm^{-1}) υ: 3333-3453 (NH_2), 2223 (CN). ^{1}H NMR (300 MHz, $CDCl_3$) δ_H: 2.85 (s, 3H, CH_3), 4.88 (s, 1H, H-pyran), 5.15 (s, 2H, -NH_2), 7.05-8.06 (m, 8H, H_{arom}). ^{13}C NMR (75 MHz, $CDCl_3$) δ_C: 25.0, 41.2, 56.7, 118.3, 120.1, 121.2, 122.3, 124.3, 126.8, 127.0, 127.5, 131.0, 135.9, 137.1, 139.0, 151.0, 155.9, 166.4. ESI-HRMS $[M+H]^+$ calcd for $(C_{20}H_{15}ClN_3O)^+$ 348.0901, found 348.0909.

Compound (2c): White solid, yield: 85%, mp: 238-240 °C (EtOH); IR (KBr, cm^{-1}) υ: 3330-3446 (NH_2), 2219 (CN). ^{1}H NMR (300 MHz, $CDCl_3$) δ_H: 2.30 (s, 3H, CH_3-Ph), 2.60 (s, 3H, CH_3), 4.79 (s, 1H, H-pyran), 5.92 (s, 2H, -NH_2), 7.05-8.06 (m, 8H, H_{arom}). ^{13}C NMR (75 MHz, $CDCl_3$) δ_C: 20.8, 24.3, 41.3, 59.2, 117.9, 120.0, 121.2, 122.2, 124.5, 126.5, 127.6, 128.4, 135.8, 136.0, 137.0, 137.3, 151.0, 155.8, 166.3. ESI-HRMS $[M+H]^+$ calcd for $(C_{21}H_{18}N_3O)^+$ 328.1410, found 328.1416.

Compound (2d): White solid, yield: 70%, mp: 235-237 °C (EtOH); IR (KBr, cm^{-1}) υ: 3335-3459 (NH_2), 2226 (CN). ^{1}H NMR (300 MHz, $CDCl_3$) δ_H: 2.80 (s, 3H, CH_3), 3.80 (s, 3H, -OCH_3), 4.75 (s, 1H, H-pyran), 5.78 (s, 2H, -NH_2), 7.01-8.26 (m, 8H, H_{arom}). ^{13}C NMR (75 MHz, $CDCl_3$) δ_C: 25.0, 41.2, 53.1, 59.1, 115.0, 118.1, 119.9, 121.2, 122.4, 124.4, 127.5, 129.6, 132.8, 135.8, 137.1, 151.1, 155.9, 159.0,

166.3. ESI-HRMS $[M+H]^+$ calcd for $(C_{21}H_{18}N_3O_2)^+$ 344.3863, found 344.3867.

General experimental way for the preparation of triazolopyrimidopyrano[3,2-*h*]quinolines 4a-f. A solution of imidates **3a-b** and some substituted hydrazides were dissolved in dry DMF, then subjected to microwave irradiation at 350 W for 5 to 9 min. Subsequently, it was poured into ice water. The obtained precipitate was recuperated by filtration, washed with water, dried and recrystallized from EtOH to afford compounds **4a-f**.

Compound (4a): White solid, yield: 75%, mp: 252-254 °C (EtOH); IR (KBr, cm^{-1}) υ: 1610 (C=N), 1490 (C-O), 1445 (C=C). ^{1}H NMR (300 MHz, $CDCl_3$) δ_H: 2.55 (s, 3H, CH_3-triazole), 2.88 (s, 3H, CH_3), 5.81 (s, 1H, H-pyran), 7.13-8.01 (m, 9H, H_{arom}), 9.04 (s, 1H, H-pyrimidine). ^{13}C NMR (75 MHz, $CDCl_3$) δ_C: 14.2, 25.1, 43.6, 118.3, 119.8, 121.4, 122.0, 125.4, 126.6, 127.8, 128.2, 129.4, 135.4, 136.8, 137.5, 143.0, 147.1, 150.2, 152.6, 155.9, 166.6. ESI-HRMS $[M+H]^+$ calcd for $(C_{23}H_{18}N_5O)^+$ 380.1524, found 380.1533.

Compound (4b): White solid, yield: 75%, mp: 260-262 °C (EtOH); IR (KBr, cm^{-1}) υ: 1621 (C=N), 1496 (C-O), 1450 (C=C). ^{1}H NMR (300 MHz, $CDCl_3$) δ_H: 2.87 (s, 3H, -CH_3), 5.94 (s, 1H, H-pyran), 7.16-8.05 (m, 14H, H_{arom}), 9.13 (s, 1H, H-pyrimidine). ^{13}C NMR (75 MHz, $CDCl_3$) δ_C: 25.1, 43.6, 118.3, 119.8, 121.4, 122.0, 125.4, 126.6, 127.3, 127.8, 128.2, 129.1, 129.3, 131,2, 133.0, 135.4, 136.8, 137.5, 143.1, 147.1, 150.2, 155.9, 160.0, 166.6. ESI-HRMS $[M+H]^+$ calcd for $(C_{28}H_{20}N_5O)^+$ 442.1665, found 442.1674.

Compound (4c): White solid, yield: 78%, mp: 255-257 °C (EtOH); IR (KBr, cm^{-1}) υ: 2260 (CN), 1611 (C=N), 1486 (C-O), 1443 (C=C). ^{1}H NMR (300 MHz, $CDCl_3$) δ_H: 2.89 (s, 3H, CH_3), 4.01 (s, 2H, -CH_2-CN), 5.86 (s, 1H, H-pyran), 7.18-8.05 (m, 9H, H_{arom}), 9.14 (s, 1H, H-pyrimidine). ^{13}C NMR (75 MHz, $CDCl_3$) δ_C: 18.1, 25.1, 43.1, 117.5, 118.3, 119.8, 121.4, 122.0, 125.4, 126.6, 127.3, 128.3, 129.3, 135.4, 136.6, 137.5, 143.1, 146.3, 147.1, 150.2, 155.9, 166.5. ESI-HRMS $[M+H]^+$ calcd for $(C_{24}H_{17}N_6O)^+$ 405.1471, found 405.1485.

Compound (4d): White solid, yield: 82%, mp: 248-250 °C (EtOH); IR (KBr, cm^{-1}) υ: 1617 (C=N), 1475 (C-O), 1450 (C=C). ^{1}H NMR (300 MHz, $CDCl_3$) δ_H: 2.57 (s, 3H, CH_3-triazole), 2.93 (s, 3H, CH_3), 5.84 (s, 1H, H-pyran), 7.20-8.08 (m, 8H, H_{arom}), 9.07 (s, 1H, H-pyrimidine), ^{13}C NMR (75 MHz, $CDCl_3$) δ_C: 14.2, 25.1, 43.5, 118.1, 119.9, 121.1, 121.9, 125.4, 127.8, 129.5, 129.9, 132.3, 134.5, 136.4, 137.6, 142.0, 147.2, 150.4, 152.6, 156.0, 166.6. ESI-HRMS $[M+H]^+$ calcd for $(C_{23}H_{17}ClN_5O)^+$ 414.1114, found 414.1121.

Compound (4e): White solid, yield: 75%, mp: 266-268 °C (EtOH); IR (KBr, cm^{-1}) υ: 1615 (C=N), 1471 (C-O), 1456 (C=C). ^{1}H NMR (300 MHz, $CDCl_3$) δ_H: 2.88 (s, 3H, CH_3), 5.93 (s, 1H, H-pyran), 7.22-8.27 (m, 13H, H_{arom}), 9.14 (s, 1H, H-pyrimidine). ^{13}C NMR (75 MHz, $CDCl_3$) δ_C: 25.0, 42.9, 118.2, 119.8, 121.2, 122.0, 125.5, 127.3, 127.7, 129.5, 129.8, 130.2, 132.0, 132.5, 133.0, 134.5, 136.7, 137.5, 141.4, 147.4, 150.6, 159.3, 156.3, 166.6. ESI-HRMS $[M+H]^+$ calcd for $(C_{28}H_{19}ClN_5O)^+$ 476.1270, found 476.1278.

Compound (4f): White solid, yield: 75%, mp: 260-262 °C (EtOH); IR (KBr, cm^{-1}) υ: 2257 (CN), 1610 (C=N), 1480 (C-O), 1445 (C=C). ^{1}H NMR (300 MHz, $CDCl_3$) δ_H: 2.88 (s, 3H, CH_3), 3.99 (s, 2H, -CH_2-CN), 5.84 (s, 1H, H-pyran), 7.20-8.05 (m, 8H, H_{arom}), 9.13 (s, 1H, H-pyrimidine). ^{13}C NMR (75 MHz, $CDCl_3$) δ_C: 18.6, 25.0, 42.9, 117.9, 118.2, 119.8, 121.2, 122.0, 125.5, 127.7, 129.5, 129.8, 132.5, 134.5, 136.7, 137.5, 141.3, 146.7, 147.4, 150.6, 156.3, 166.5. ESI-HRMS $[M+H]^+$ calcd for $(C_{24}H_{16}ClN_6O)^+$ 439.1065, found 439.1077.

General procedure for the preparation of compounds 5a-c and 6a-h. A mixture of 2-cyanomethyl derivatives **4a-b** and some arylaldehydes or salicylic aldehydes in EtOH and few drops of piperidine was refluxed, and the evolution of the reaction was checked by TLC. After the reaction was completed, the temperature of the reaction mixture was lowered to 25 °C. The precipitate thus produced was filtered and washed several times from EtOH to give **5a-c** or **6a-h.**

Compound (5a): White solid, yield: 72%, mp: >300 °C (EtOH); IR (KBr, cm^{-1}) υ: 3330 (-NH-), 1630 (C=N), 1459 (C=C). ^{1}H NMR (300 MHz, DMSO-d_6) δ_H: 2.55 (s, 3H, -CH_3), 5.45 (s, 1H, H-pyran), 7.10-8.10 (m, 15H, H_{arom}+ -NH), 9.10 (s, 1H, H-pyrimidine). ^{13}C NMR (75 MHz, DMSO-d_6) δ_C: 25.1, 43.1, 114.0, 115.7, 118.2, 120.1, 120.9, 121.1, 121.4, 126.5, 127.8, 128.2, 128.4, 128.7, 129.2, 129.5, 129.6, 135.4, 136.3, 136.7, 137.1, 143.1, 147.1, 147,8, 150.1, 151.6, 153.2, 160.4, 162.1. ESI-HRMS $[M+H]^+$ calcd for $(C_{31}H_{21}N_6O_2)^+$ 509.1715, found 509.1725.

Compound (5b): White solid, yield: 76%, mp: >300 °C (EtOH); IR (KBr, cm^{-1}) υ: 3325 (-NH-), 1625 (C=N), 1450 (C=C). ^{1}H NMR (300 MHz, DMSO-d_6) δ_H: 2.48 (s, 3H, -CH_3), 5.38 (s, 1H, H-pyran), 7.10-8.15 (m, 14H, H_{arom}+ -NH), 9.14 (s, 1H, H-pyrimidine). ^{13}C NMR (75 MHz, DMSO-d_6) δ_C: 24.6, 44.2, 114.1, 115.0, 118.1, 119.8, 120.9, 121.1, 121.4, 120.8, 125.4, 127.4, 128.9, 129.6, 129.8, 130.1, 132.1, 134.5, 136.2, 136.9, 137.3, 142.6, 147.1, 147.7, 150.8, 154.1, 155.4, 160.5, 162.3. ESI-HRMS $[M+H]^+$ calcd for $(C_{31}H_{20}N_6O_2)^+$ 587.0812, found 587.0812.

Compound (5c): White solid, yield: 79%, mp: >300 °C (EtOH); IR (KBr, cm^{-1}) υ: 3335 (-NH-), 1625 (C=N), 1450 (C=C). ^{1}H NMR (300 MHz, DMSO-d_6) δ_H: 2.43 (s, 3H, -CH_3), 5.33 (s, 1H, H-pyran), 7.11-8.25 (m, 14H, H_{arom}+ -NH), 9.15 (s, 1H, H-pyrimidine). ^{13}C NMR (75 MHz, DMSO-d_6) δ_C: 24.5, 44.0, 114.1, 116.1, 118.3, 119.6, 121.0, 121.3, 121.2, 124.0, 125.6, 127.3, 128.9, 129.2, 129.8, 131.6, 134.6, 136.4, 136.7, 137.3, 146.3, 147.1, 147.5, 149.3, 150.9, 154.2, 155.4, 160.5, 162.2. ESI-HRMS $[M+H]^+$ calcd for $(C_{31}H_{20}N_7O_4)^+$ 554.1535, found 554.1545.

Compound (6a): White solid, yield: 70%, mp: 294-296 °C (EtOH); IR (KBr, cm^{-1}) υ: 2220 (CN), 1620 (C=N), 1450 (C=C). ^{1}H NMR (300 MHz, DMSO-d_6) δ_H: 2.60 (s, 3H, -CH_3), 5.60 (s, 1H, H-pyran), 7.10-8.05 (m, 14H, H_{arom}), 9.10 (s, 1H, H-pyrimidine), 9.20 (s, 1H, $H_{3'}$). ^{13}C NMR (75 MHz, DMSO-d_6) δ_C: 24.1, 42.0, 107.1, 118.0, 119.0, 119.8, 120.9, 121.6, 125.9, 126.3, 127.2, 127.9, 128.2, 128.4, 128.6, 129.2, 134.2, 135.3, 136.6, 137.2, 143.2, 147.1, 147.5, 150.4, 153.5, 155.4, 161.8. ESI-HRMS $[M+H]^+$

calcd for $(C_{31}H_{21}N_6O)^+$ 493.1770, found 493.1777.

Compound (6b): White solid, yield: 73%, mp: 295-297 °C (EtOH); IR (KBr, cm^{-1}) υ: 2225 (CN), 1618 (C=N), 1454 (C=C). ^{1}H NMR (300 MHz, DMSO-*d*$_6$) δ_H: 2.30 (s, 3H, CH_3-Ph), 2.58 (s, 3H, -CH_3), 5.65 (s, 1H, H-pyran), 7.10-8.05 (m, 13H, H_{arom}), 9.12 (s, 1H, H-pyrimidine), 9.15 (s, 1H, $H_{3'}$). ^{13}C NMR (75 MHz, DMSO-*d*$_6$) δ_C: 21.1, 24.0, 43.2, 107.7, 118.1, 118.8, 119.7, 120.7, 121.6, 125.8, 126.3, 127.2, 128.2, 128.6, 128.8, 129.3, 132.2, 134.2, 136.8, 136.9, 137.5, 143.2, 147.0, 147.4, 150.7, 153.2, 155.2, 161.7. ESI-HRMS $[M+H]^+$ calcd for $(C_{32}H_{23}N_6O)^+$ 507.1935, found 507.1941.

Compound (6c): White solid, yield: 78%, mp: 293-295 °C (EtOH); IR (KBr, cm^{-1}) υ: 2230 (CN), 1628 (C=N), 1460 (C=C). ^{1}H NMR (300 MHz, DMSO-*d*$_6$) δ_H: 2.51 (s, 3H, -CH_3), 3.60 (s, 3H, -OCH_3-Ph) 5.54 (s, 1H, H-pyran), 7.11-8.30 (m, 13H, H_{arom}), 9.10 (s, 1H, H-pyrimidine), 9.20 (s, 1H, $H_{3'}$). ^{13}C NMR (75 MHz, DMSO-*d*$_6$) δ_C: 24.2, 44.0, 55.8, 107.0, 114.0, 118.1, 118.9, 119.7, 121.2, 121.5, 125.5, 126.3, 127.3, 127.5, 128.1, 129.2, 130.2, 134.5, 136.5, 137.0, 143.1, 147.0, 147.2, 151.4, 153.4, 156.8, 159.7, 162.0. ESI-HRMS $[M+H]^+$ calcd for $(C_{31}H_{20}ClN_6O)^+$ 527.1380, found 527.1389.

Compound (6d): White solid, yield: 80%, mp: 280-282 °C (EtOH); IR (KBr, cm^{-1}) υ: 2235 (CN), 1618 (C=N), 1465 (C=C). ^{1}H NMR (300 MHz, DMSO-*d*$_6$) δ_H: 2.49 (s, 3H, -CH_3), 3.10 (s, 6H, -N-$(CH_3)_2$), 5.42 (s, 1H, H-pyran), 7.01-8.40 (m, 13H, H_{arom}), 9.13 (s, 1H, H-pyrimidine), 9.22 (s, 1H, $H_{3'}$). ^{13}C NMR (75 MHz, DMSO-*d*$_6$) δ_C: 24.6, 41.1, 43.0, 107.4, 111.9, 118.1, 1187, 119.7, 120.9, 121.5, 124.6, 125.5, 126.3, 127.3, 128.0, 129.0, 129.9, 134.6, 136.4, 137.5, 143.0, 147.2, 147.4, 150.4, 150.9, 153.5, 155.9, 161.8. ESI-HRMS $[M+H]^+$ calcd for $(C_{33}H_{26}N_7O)^+$ 536.2123, found 536.2133.

Compound (6e): White solid, yield: 68%, mp: 297-299 °C (EtOH); IR (KBr, cm^{-1}) υ: 2235 (CN), 1620 (C=N), 1458 (C=C). ^{1}H NMR (300 MHz, DMSO-*d*$_6$) δ_H: 2.50 (s, 3H, -CH_3), 5.57 (s, 1H, H-pyran), 7.17-8.34 (m, 13H, H_{arom}), 9.14 (s, 1H, H-pyrimidine), 9.20 (s, 1H, $H_{3'}$). ^{13}C NMR (75 MHz, DMSO-*d*$_6$) δ_C: 24.0, 43.6, 107.5, 117.9, 118.7, 119.8, 121.0, 121.6, 125.5, 127.3, 127.8, 128.4, 128.6, 129.1, 129.6, 131.8, 134.5, 135.4, 137.0, 137.1, 141.6, 147.0, 147.2, 150.8, 153.6, 156.0, 161.8. ESI-HRMS $[M+H]^+$ calcd for $(C_{32}H_{23}N_6O_2)^+$ 523.1865, found 523.1873.

Compound (6f): White solid, yield: 70%, mp: 290-292 °C (EtOH); IR (KBr, cm^{-1}) υ: 2228 (CN), 1620 (C=N), 1455 (C=C). ^{1}H NMR (300 MHz, DMSO-*d*$_6$) δ_H: 2.37 (s, 3H, CH_3-Ph), 2.51 (s, 3H, -CH_3), 5.57 (s, 1H, H-pyran), 7.10-8.20 (m, 12H, H_{arom}), 9.10 (s, 1H, H-pyrimidine), 9.22 (s, 1H, $H_{3'}$). ^{13}C NMR (75 MHz, DMSO-*d*$_6$) δ_C: 21.8, 25.0, 43.7, 107.4, 117.9, 118.7, 119.9, 121.1, 121.5, 125.7, 127.1, 128.5, 129.0, 129.3, 129.7, 131.6, 132.3, 134.8, 136.8, 137.4, 137.8, 141.7, 147.0, 147.4, 150.8, 153.7, 155.6, 162.0. ESI-HRMS $[M+H]^+$ calcd for $(C_{32}H_{22}ClN_6O)^+$ 541.1547, found 541.1550.

Compound (6g): White solid, yield: 75%, mp: 294-296 °C (EtOH); IR (KBr, cm^{-1}) υ: 2233 (CN), 1625 (C=N), 1455 (C=C). ^{1}H NMR (300 MHz, DMSO-*d*$_6$) δ_H: 2.55 (s, 3H, -CH_3), 3.67 (s, 3H, -OCH_3-Ph), 5.50 (s, 1H, H-pyran), 7.12-8.11 (m, 12H, H_{arom}), 9.14 (s, 1H, H-pyrimidine), 9.25 (s, 1H, $H_{3'}$). ^{13}C NMR

(75 MHz, DMSO-d_6) δ_C: 24.3, 44.1, 55.7, 107.7, 115.8, 118.1, 118.7, 119.8, 121.1, 121.4, 125.6, 127.1, 127.7, 129.1, 129.7, 130.2, 131.9, 134.3, 136.6, 137.3, 141.3, 147.0, 147.3, 150.8, 153.5, 155.8, 159.7, 161.9. ESI-HRMS $[M+H]^+$ calcd for $(C_{32}H_{21}ClN_6O_2)^+$ 556.1430, found 556.1437.

Compound (6h): White solid, yield: 78%, mp: 284-286 °C (EtOH); IR (KBr, cm^{-1}) υ: 2235 (CN), 1620 (C=N), 1450 (C=C). ^{1}H NMR (300 MHz, DMSO-d_6) δ_H: 2.50 (s, 3H, -CH_3), 3.07 (s, 6H, -N-(CH_3)$_2$), 5.48 (s, 1H, H-pyran), 7.01-8.01 (m, 12H, H_{arom}), 9.16 (s, 1H, H-pyrimidine), 9.21 (s, 1H, $H_{3'}$). ^{13}C NMR (75 MHz, DMSO-d_6) δ_C: 24.1, 40.7, 43.7, 107.7, 110.9, 118.0, 118.9, 119.8, 121.1, 121.3, 124.8, 125.6, 127.2, 129.1, 129.7, 129.9, 131.8, 134.6, 136.7, 137.0, 141.3, 147.1, 147.4, 150.1, 150.6, 153.3, 155.6, 162.1. ESI-HRMS $[M+H]^+$ calcd for $(C_{33}H_{25}ClN_7O)^+$ 570.1823, found 570.1830.

Molecular Docking Procedure. The chemical structures of the co-crystallized inhibitor (N3) and of the synthesized compounds (**4c**, **4f**, **5a-f**, and **6a-h**) were generated and optimized using ACD (3D viewer) software (http://www.filefacts.com/acd3d-viewer-freeware-info), where their energies were minimized. The crystal structure of SARS-CoV-2 M^{pro} (PDB: 6LU7) was obtained from the RSCB data bank (https://www.rcsb.org). The inhibitor ligand and water molecules were removed from the protein before use, after which, polar hydrogens and Kollman charges were introduced. Therefore, the grid box (40 x 40 x 40 points), spacing of 1.0 Å and centered with coordinates x: -11.993, y: 15.425, and z: 65.951, was designed according to the binding position of N3 in the binding site of the target protein. Molecular Docking studies of compounds **4c**, **4f**, **5a-f** and **6a-h** as well as N3, were accomplished with AutoDock Vina software.[51] Enzyme-molecule interactions were presented and explained using the Biovia Discovery Studio Visualizer (BIOVIA, D. S. (2017)).

ACKNOWLEDGEMENTS

This research was supported by the Deanship of Scientific Research, Imam Mohammad Ibn Saud Islamic University (IMSIU), Saudi Arabia, Grant No. (21-13-18-063).

REFERENCES

1. J. T. Wu, K. Leung, and G. M. Leung, *Lancet*, 2020, **395**, 689.
2. D. S. Hui, E. I. Azhar, T. A. Madani, F. Ntoumi, R. Kock, O. Dar, G. Ippolito, T. D. Mchugh, Z. A. Memish, C. Drosten, A. Zumla, and E. Petersen, *Int. J. Infect. Dis.*, 2020, **91**, 264.
3. R. W. DeSimone, K. S. Currie, S. A. Mitchell, J. W. Darrow, and D. A. Pippin, *Comb. Chem. High Throughput Screen.*, 2004, **7**, 473.
4. C. D. Duarte, E. J. Barreiro, and C. A. M. Fraga, *Mini-Rev. Med. Chem.*, 2007, **7**, 1108.
5. F. Mao, J. Yan, J. Li, X. Jia, H. Miao, Y. Sun, L. Huang, and X. Li, *Org. Biomol. Chem.*, 2014, **12**, 5936.

6. V. Moret, Y. Laras, T. Cresteil, G. Aubert, D. Q. Ping, C. Di, M. Barthélémy-Requin, C. Béclin, V. Peyrot, D. Allegro, A. Rolland, F. De Angelis, E. Gatti, P. Pierre, L. Pasquini, E. Petrucci, U. Testa, and J. L. Kraus, *Eur. J. Med. Chem*., 2009, **44**, 558.
7. X. Y. Jin, H. Chen, D.-D. Li, A.-L. Li, W.-Y. Wang, and W. Gu, *J. Enzyme Inhib. Med. Chem.*, 2019, **34**, 955.
8. S. H. Chan, C. H. Chui, S. W. Chan, S. H. Kok, D. Chan, M. Y. Tsoi, P. H. Leung, A. K. Lam, A. S. Chan, K. H. Lam, and J. C. Tang, *ACS Med. Chem. Lett*., 2013, **4**, 170.
9. S. M. Cohen, A. Agrawal, J. Desoto, Y. Pommier, and K. Maddali, *PCT Int. Appl., WO 2012106534 A2*, 2012, 20120809.
10. E. Serrao, B. Debnath, H. Otake, Y. Kuang, F. Christ, Z. Debyser, and N. Neamati, *J. Med. Chem.*, 2013, **56**, 2311.
11. A. F. Eweas, G. Allam, A. S. Abuelsaad, A. H. Alghamdi, and I. A. Maghrabi, *Bioorg. Chem.*, 2013, **46**, 17.
12. M. J. Cheng, K. H. Lee, I. L. Tsai, and I. S. Chen, *Bioorg. Med. Chem*., 2005, **13**, 5915.
13. R. Kaur and K. Kumar, *Eur. J. Med. Chem*., 2021, **215**, 113220.
14. Y. H. Kim, N. G. Kim, J. G. Lim, C. Park, and H. Kim, *Am. J. Pathol.*, 2001, **158**, 655.
15. S. W. Carmack, R. M. Genta, C. M. Schuler, and M. H. Saboorian, *Am. J. Gastroenterol*., 2009, **104**, 1524.
16. A. F. Goddard, R. Badreldin, D. M. Pritchard, M. M. Walker, and B. Warren, *Gut*, 2010, **59**, 1270.
17. F. Qin, X. Huang, and P. Ren, *J. Gastroenterol. Hepatol.*, 2009, **24**, 1320.
18. S. M. Mahdavi, A. Habibi, H. Dolati, S. M. Shahcheragh, S. Sardari, and P. Azerang, *Iran. J. Pharm. Res.*, 2018, **17**, 1229.
19. M. Debbabi, V. D. Nimbarte, S. Chekir, S. Chortani, A. Romdhane, and H. Ben Jannet, *Bioorg. Chem*., 2019, **82**, 129.
20. A. Hajlaoui, M. Laajimi, M. Znati, H. Ben Jannet, and A. Romdhane, *J. Mol. Struct*., 2021, **1237**, 130346.
21. A. B. Saïd, A. Romdhane, N. Elie, D. Touboul, H. Ben Jannet, and J. Bouajila, *J. Enzyme Inhib. Med. Chem*., 2016, **31**, 1277.
22. H. Sirous, A. Fassihi, S. Brogi, G. Campiani, F. Chirist, Z. Debyser, S. Gemma, S. Butini, G. Chemi, A. Grillo, R. Zabihollahi, M. R. Aghasadeghi, L. Saghaie, and H. R. Memarian, *Med. Chem.*, 2019, **15**, 755.
23. C.-A. Geng, X.-Y. Huang, Y.-B. Ma, X.-M. Zhang, and J.-J. Chen, *Bioorg. Med. Chem. Lett*., 2015, **25**, 1568.
24. C. Xiu, Z. Hua, B. S. Xiao, W. J. Tang, H. P. Zhou, and X. H. Liu, *Expert Opin. Ther. Pat*., 2017, **27**,

1031.

25. A. Romdhane, A. B. Said, M. Cherif, and H. Ben Jannet, *Med. Chem. Res*., 2016, **25**, 1358.
26. A. M. Mohamed, H. R. M. Al-Qalawi, W. A. El-Sayed, W. A. A. Arafa, M. S. Alhumaimess, and A. K. Hassan, *Acta Pol. Pharm*., 2015, **72**, 307.
27. M. A. A. Radwan, F. M. Alminderej, H. E. M. Tolan, and H. M. Awad, *J. App. Pharm. Sci*., 2020, **10**, 12.
28. M. A. Phillips, R. Gujjar, N. A. Malmquist, J. White, F. El Mazouni, J. Baldwin, and P. K. Rathod, *J. Med. Chem*., 2008, **51**, 3649.
29. J. Desantis, S. Massari, A. Corona, A. Astolfi, S. Sabatini, G. Manfroni, D. Palazzotti, V. Cecchetti, C. Pannecouque, E. Tramontano, and O. Tabarrini, *Molecules*, 2020, **25**, 1183.
30. B. Huang, D. Kang, Y. Tian, D. Daelemans, E. De Clercq, C. Pannecoupe, P. Zhan, and X. Liu, *Chem. Biol. Drug Des*., 2021, **97**, 67.
31. J. Zhao, Y. Zhang, M. Wang, Q. Liu, X. Lei, M. Wu, S. Guo, D. Yi, Q. Li, L. Ma, Z. Liu, F. Guo, J. Wang, X. Li, Y. Wang, and S. Cen, *ACS Infect. Dis*., 2021, **7**, 1535.
32. R. M. Mohareb and N. Y. M. Abdo, *J. Iran. Chem. Soc.*, 2021, https:///doi.org/10.1007/s13738-021-0366-x.
33. M. C. Pismataro, T. Felicetti, C. Bertagnin, M. G. Nizi, A. Bonomini, M. L. Barreca, V. Cecchetti, D. Jochmans, S. De Jonghe, J. Neyts, A. Loregian, O. Tabarrini, and S. Massari, *Eur. J. Med. Chem*., 2021, **221**, 113494.
34. M. Horchani, G. D. Sala, A. Caso, F. D'Aria, G. Esposito, I. Laurenzana, C. Giancola, V. Costantino, H. Ben Jannet, and A. Romdhane, *Int. J. Mol. Sci.*, 2021, **22**, 2742.
35. S. Chortani, M. Horchani, M. Znati, N. Issaoui, H. Ben Jannet, and A. Romdhane, *J. Mol. Struct*., 2021, **1230**, 129920.
36. M. Znati, M. Horchani, L. Latapie, H. Ben Jannet, and J. Bouajila, *J. Mol. Struct*., 2021, **1246**, 131216.
37. M. Horchani, N. V. Heise, S. Hoenke, R. Csuk, A. H. Harrath, H. Ben Jannet, and A. Romdhane, *Int. J. Mol. Sci.*, 2021, **22**, 10258.
38. A. B. Said, A. Rahmouni, M. D. Ramadi, A. Romdhane, and H. Ben Jannet, *J. Tun. Chem. Soc*., 2017, **19**, 94.
39. M. Cherif, M. Debbabi, S. Chortani, A. Romdhane, and H. Ben Jannet, *Turk. J. Chem*., 2018, **42**, 1623.
40. M. R. N. Jamal, S. Mashkouri, and A. Sharif, *Mol. Divers.*, 2010, **14**, 473.
41. A. Y. Hassan, *Phosphorus, Sulfur Silicon Relat. Elem.*, 2009, **184**, 2856.
42. H. Bayrak, A. Demirbas, H. Bektas, S. A. Karaoglu, and N. Demirbas, *Turk. J. Chem*.,

2010, **34**, 835.

43. X. Yang, H. Yu, Y. Xu, and L. Shao, *J. Org. Chem*., 2018, **83**, 9682.
44. T. Deligeorgiev, T. Tsvetkova, S. Kaloyanova, D. Ivanova, and I. Timtcheva, *Color. Technol*., 2010, **126**, 209.
45. R. M. Mohareb, A. E. M. Abdallah, and A. A. Mohamed, *Chem. Pharm. Bull*., 2018, **66**, 309.
46. M. Lončarić, D. Gašo-Sokač, S. Jokić, and M. Molnar, *Biomolecules*, 2020, **10**, 151.
47. L. Muralidhar and C. R. Girija, *J. Saudi Chem. Soc*., 2014, **18**, 541.
48. K. van Beurden, S. de Koning, D. Molendijk, and J. van Schijndel, *Green Chem. Lett. Rev*., 2020, **13**, 349.
49. R. Soltane, A. Chrouda, A. Mostafa, A. A. Al-Karmalawy, K. Chouaïb, A. Dhahri, R. Adel Pashameah, A. Alasiri, O. Kutkat, M. Shehata, H. Ben Jannet, J. Gharbi, and M. A. Ali, *Pathogens*, 2021, **10**, 623.
50. A. H. Arshia, S. Shadravan, A. Solhjoo, A. h. Sakhteman, and A. Sami, *Comput. Biol. Med.*, 2021, **139**, 104967.
51. O. Trott and A. J. Olson, *J. Comput. Chem*., 2010, **31**, 455.